The metallophilic interaction between cyclometalated complexes: photobiological applications

Zhou, X.

2

The two isomers of a cyclometalated palladium sensitizer show distinct photodynamic properties in cancer cells

This report demonstrates that changing the place of the carbon-metal bond in a polypyridyl cyclopalladated complex, i.e. going from ***PdL*^{1}** *(N^N^C^N) to* ***PdL*^{2}** *(N^N^N^C), dramatically influences the photodynamic therapeutic ability of the complex in cancer cells. This effect is attributed to the significant difference in absorbance and singlet oxygen quantum yields of the two isomers.*

This chapter was published as a communication: X.-Q. Zhou, A. Busemann, M. Meijer, M. A. Siegler and S. Bonnet*, ***Chem. Comm.***, 2019, **55**, 4695-4698.

2.1 Introduction

The success of cisplatin, a milestone drug in the treatment of cancers, stimulated the generation of many platinum-based anticancer drugs,[1-3] three of which (carboplatin, oxaliplatin and nedaplatin) are approved worldwide. However, the unselective covalent binding of cisplatin with DNA in cancer cells and healthy cells results in serious side effects and drug resistance, which has encouraged the development of anticancer drugs based on alternative metals.[4-9] In this regards, palladium(II) complexes have been proposed as potential metal-based anticancer drugs for their similar d^8 coordination sphere and square-planar structure, compared to platinum(II) complexes.[10, 11] One of them, called padeliporfin or WST11, was recently approved for photodynamic therapy (PDT) of prostate cancer.[12] PDT is a form of light-activated cancer therapy. It emerges as a more patient-friendly approach due to the controlled toxicity effect and low invasiveness of light irradiation.[13-17] In PDT, a photosensitizing agent (PS) is irradiated by visible light at the tumor site, where it generates cytotoxic reactive oxygen species (ROS), which induce cancer cell death.[18] Polypyridyl metal complexes typically form excellent PDT sensitizers, provided they strongly absorb visible light.[19, 20] The light absorption properties of such complexes can be tuned by changing the metal or the ligands. Critically, good photosensitizers should be photostable, which demands on the strong coordination bonds of multidentate ligands.

Recently, bioactive pincer palladium complexes with tridentate N-heterocyclic carbene ligands showed strong metal-carbon bonds and tunable physicochemical properties.[10, 21-24] However, the intracellular substitution of remaining monodentate ligand makes speciation in biological medium and mode-of-action complicated to understand. In addition, due to the smaller ionic radius of Pd^{2+} ions, Pd-ligand bonds are longer and more labile than their Pt-ligand analogues,[25] so that anticancer drugs based on palladium(II) are still comparatively rare.[6] To overcome these drawbacks, we investigated the design and properties of palladium(II) PDT sensitizers built from single tetradentate cyclometalating ligands, which are expected to be more stable in biological medium compared with the tridentate N-heterocyclic carbene ligands. Cyclometalation was considered for different reasons. First, the strong Pd-C bond can stabilize these compounds in biological medium. Second, the lower charge introduced by the cyclometalated ligand can improve the lipophilicity and cellular uptake of the metal complexes.[7, 26] Third, the presence of a Pd-C bond should in principle lead to a bathochromic shift of the visible absorption bands of the metal complex, which is key for PDT applications.[27] In polypyridyl metal complexes, introducing a metal-carbon bond usually generates a series of

isomers that might have different properties. Herein we investigated two novel cyclopalladated palladium isomers **PdL^1** (**H$_2$L^1** = N-(3-(pyridin-2-yl)phenyl)-[2,2'-bipyridin]-6-amine) and **PdL^2** (**H$_2$L^2** = N-(6-phenylpyridin-2-yl)-[2,2'-bipyridin]-6-amine) (Scheme 2.1a). In **PdL^1**, the Pd-C bond was introduced in a pyridyl group that is adjacent to the non-bonded nitrogen bridge of the ligand, while in **PdL^2** it is introduced in one of the terminal aromatic rings.

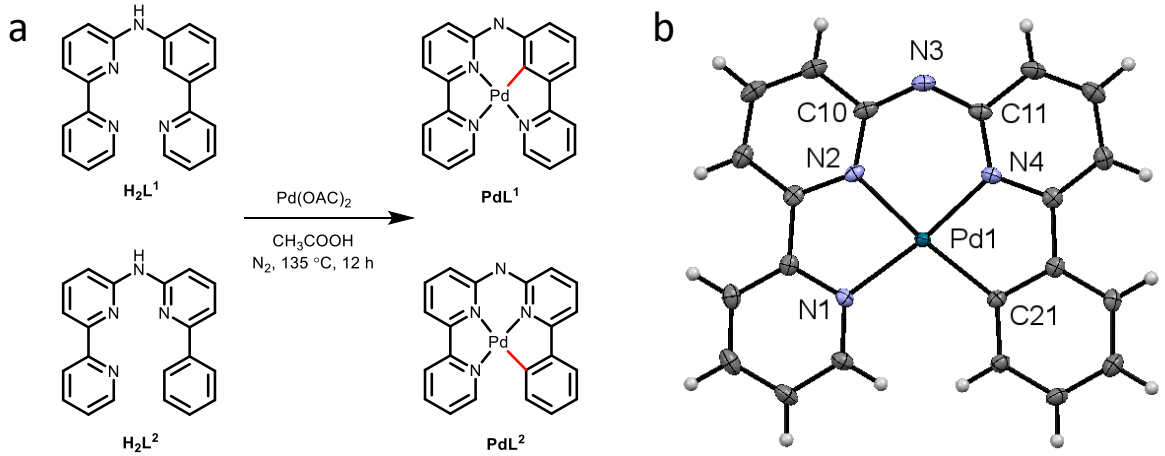

Scheme 2.1 *(a) Synthesis of **PdL^1** and **PdL^2**; (b) Displacement ellipsoid plot (50% probability level) of **PdL^2** at 110(2) K (bond distance: Pd-N1 2.060(3) Å, Pd-N2 2.028(4) Å, Pd-N4 1.988(3) Å, Pd-C21 2.017(4) Å); angle: N4-Pd1-C21 81.99(15)°, N4-Pd1-N2 92.66(16)°, C21-Pd1-N2 174.65(18)°, N4-Pd1-N1 172.2(2)°, C21-Pd1-N1 105.02(17)°, N2-Pd1-N1 80.33(13)°).*

2.2 Results and discussion

The ligands **H$_2$L^1** and **H$_2$L^2** were synthesized by Buchwald–Hartwig coupling reactions (Scheme AI.1).[28-30] Palladation of the ligands was obtained in more than 90% yield by reacting in acetic acid the corresponding ligands with palladium(II) acetate (Scheme AI.1). ^{1}H NMR spectra of both Pd complexes, as well as their infrared spectra (IR, Figure AI.1), did not show any peak or vibration mode characteristic for a secondary amine bridge, which altogether suggested deprotonation upon coordination. According to ^{13}C-APT NMR, the ligands **H$_2$L^1** and **H$_2$L^2** have six quaternary carbon peaks, while their palladium complexes have seven, demonstrating that cyclometallation did occur. Altogether **PdL^1** and **PdL^2** appear to be neutral complexes; their identical HRMS data also demonstrated they are coordination isomers.

Vapor diffusion of diethyl ether into a methanol solution of **PdL^2** was used to yield the red rectangular crystals suitable for X-ray structure determination (Table AI.1 and Scheme 1b). **PdL^2** crystallized in the centrosymmetric $P2_1/n$ monoclinic space group. Three nitrogen and one carbon were coordinated to the palladium(II) cation, with bond lengths in the range

1.988(3)-2.028(4) Å for the three Pd-N bonds, and a Pd-C bond distance of 2.017(4) Å. The coordination sphere was slightly distorted, with a torsion angle N1-N2-N4-C21 of 2.33°. τ_4, a structural parameter calculated by (360°-(α+β))/(141°), where α and β are the two greatest valence angles of the coordination sphere, [31] was 0.093 in the structure of **PdL^2**, which is typical of an essentially square planar complex. Deprotonation of the nitrogen bridge was evidenced by the shorter distance between the amine nitrogen atoms and the adjacent pyridine carbon atoms (C10-N3 = 1.353(4) Å and C11-N3 = 1.349(4)), compared to that found in metal complexes with protonated nitrogen bridges (N-C distances in the range 1.36 Å to 1.39 Å).[29, 30] Also, unlike for [Fe(Hbbpya)$(NCS)_2$] complex,[32] no residual electron density was found near the bridging N atom in the structure of **PdL^2**. Finally, the asymmetric unit contained no counter-ions. In summary, X-ray crystallography confirmed NMR and IR data, showing that **PdL^1** and **PdL^2** are neutral species because of the deprotonation of the nitrogen bridge upon coordination.

The absorption spectrum of both complexes in PBS:DMSO (1:1) solution at 310 K (Figure AI.2) presented no significant changes over 24 hours, suggesting that the complexes were thermally stable in such conditions. Similar results were obtained in cell-growing medium (Figure AI.3), demonstrating good stability in such conditions. The partition coefficients ($logP_{ow}$) of the palladium complexes were determined by the shake-flask method (Table AI.2). Log P_{ow} was lower for **PdL^1** (-0.64) than for **PdL^2** (+0.046), confirming the higher solubility of the former, compared to the latter. Their cytotoxicity was tested in lung (A549) and skin (A431) cancer cell lines, both in the dark and upon blue light activation. Low doses of blue light were chosen (455 nm, 5 min, 10.5 mW cm^{-2}, 3.2 J cm^{-2}) which have by themselves no effect on cell growth.[33] The cell growth inhibition effective concentrations (EC_{50}) of **PdL^1** and **PdL^2** are reported in Table 1, and the dose-response curves are shown in Figure 2.1 and Figure AI.4. In the dark both compounds showed significant anticancer activity, with EC_{50} around 10 μM for **PdL^1** and **PdL^2** in A549 cells, respectively. After blue light activation, **PdL^1** showed a notable 13- or 4.0-fold increase in cytotoxicity in A549 and A431, respectively; while **PdL^2** showed negligible photoindex (PI = $EC_{50,dark}/EC_{50,light}$) of 1.3 or 1.4, respectively.

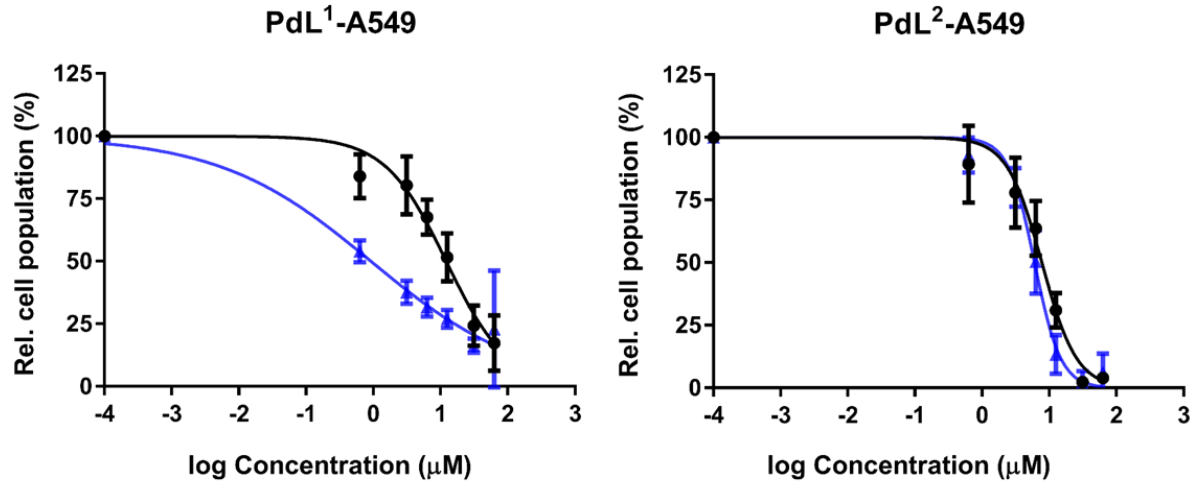

Figure 2.1 *Dose-response curves for A549 cells incubated with palladium complexes and irradiated 5 min with blue light (blue data points), or in the dark (black data points).*

Table 2.1 *The cell growing inhibition effective concentrations (EC_{50} in μM) of* ***PdL¹*** *and* ***PdL²*** *towards A549 and A431 human cancer cell lines. 95% confidence interval (CI in μM) and photoindex (PI = $EC_{50,dark}/EC_{50,light}$) are also indicated.*

Complexes		EC_{50} (μM)			
		A549	±CI	A431	±CI
PdL¹	Dark	12	+3.0 -3.0	20	+4.0 -3.0
	Light	0.9	+0.8 -0.5	5.0	+2.0 -1.0
PI		13		4.0	
PdL²	Dark	8.0	+2.0 -1.0	14	+2.0 -1.0
	Light	6.0	+0.8 -0.7	10	+1.0 -1.0
PI		1.3		1.4	

irradiation condition: 455 nm blue light, 5 min, 10.5 mW cm^{-2}, 3.2 J cm^{-2}. Data is the mean over three independent experiments.

The difference in photocytotoxicity between the two coordination isomers was quite intriguing. To investigate the reason for such difference, we first measured spectroscopically the singlet oxygen ($^1O_2$) generation quantum yield (φ_Δ) of these two isomers in CD_3OD. φ_Δ was more than twice higher for **PdL¹** (0.89) than for **PdL²** (0.38, Figure 2.2b and Table AI.3), and higher than the reference **[Ru(bpy)$_3$]Cl$_2$** (0.73).[34] However, **PdL²** was still a decent $^1O_2$ generator. In methanol, the absorbance spectra of both complexes (Figure 2.2) were similar in the 270-300 nm region; however, **PdL¹** had a much higher absorption in the blue region with λ_{max}^{abs} = 422 nm, compared to **PdL²** that absorbed in the near-UV region (λ_{max}^{abs} = 347 nm, Figure 2.2a). In

this solvent the molar absorptivity at 455 nm for **PdL^1** and **PdL^2** was 2004 M^{-1} cm^{-1} and 133 M^{-1} cm^{-1}, respectively, indicating a 15-fold enhanced absorption of **PdL^1** in the blue region, compared with **PdL^2**. Considering their similar lifetime (0.271 *vs.* 0.333 ns for the main component of their biexponential decay, Table AI.3 and Figure AI.5), the difference in $^1O_2$ generation efficiency is probably a consequence of the higher phosphorescence quantum yield for **PdL^1** (0.0017) *vs.* **PdL^2** (0.00084, Table AI.3), which points to the slower non-radiative decay pathways for the former, compared to the latter. Altogether, the dramatically higher phototoxicity of **PdL^1**, compared to **PdL^2**, seems to result from the much better absorption of blue light of **PdL^1**, coupled to its higher phosphorescence quantum yield, which leads to higher $^1O_2$ generation efficiency. Although different log P_{ow} values may lead to different cell uptake and subcellular localization for both isomers, the better photobiological properties of **PdL^1** depend, at least in part, on the much better photodynamic properties of **PdL^1**, compared to its isomer **PdL^2**.

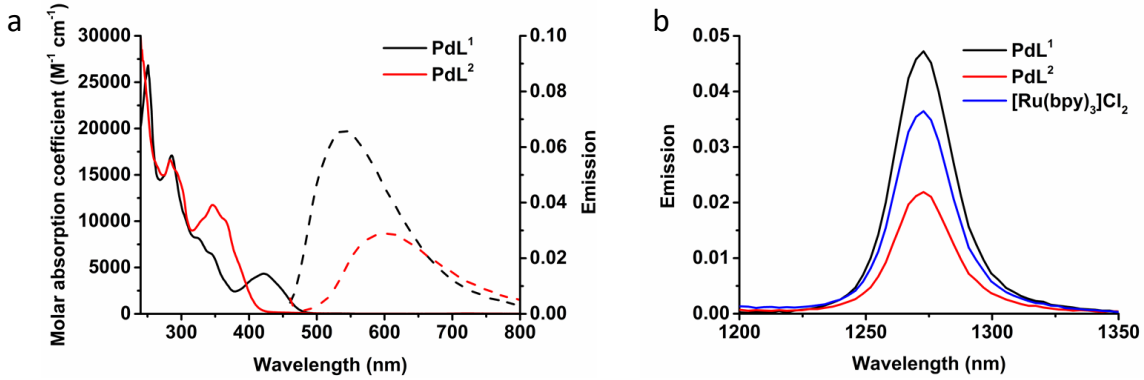

Figure 2.2 *(a) The molar absorption coefficient (solid line) and emission spectra (dash line) of* ***PdL^1*** *(black),* ***PdL^2*** *(red) in CH_3OH. (b) Singlet oxygen emission spectra of* ***[Ru(bpy)$_3$]Cl$_2$*** *(standard, blue),* ***PdL^1*** *(black),* ***PdL^2*** *(red) in CD_3OD irradiated with blue light (λ_{ex} = 450 nm, 50 mW, 200 ms).*

Density functional theory (DFT) calculations were performed to understand why **PdL^1** exhibited higher absorption in the blue domain than its isomer **PdL^2**. The nature of the highest occupied molecular orbital (HOMO) and lowest unoccupied molecular orbitals (LUMO) is highly relevant to predict the photophysical properties of metal complexes.[35-37] As shown in Figure 2.3, the HOMO and LUMO orbitals of both isomers **PdL^1** and **PdL^2** had π symmetry and were centered on the ligand, with a negligible contribution of the palladium(II) center. The bridged secondary amine is the major contributor to the HOMO of both Pd complexes, attributing for 20.4% (**PdL^1**) and 21.8% (**PdL^2**) of the electron density. The rest of the HOMO

orbital density was located in the aromatic rings directly connected to the nitrogen bridge. By contrast, the LUMO orbitals for both complexes were centered on the bipyridyl fragment. This suggested that the lowest energy absorption band of both palladium complexes should be of ligand-to-ligand charge transfer character, from the amine to the bipyridyl.

The calculated energies of HOMOs, LUMOs and energy gaps are listed in Table S4. The HOMO of **PdL^1** was significantly higher in energy than that of **PdL^2**, indicating the higher electron-donating effect of the negatively charged carbon atom of **PdL^1**, compared with that of **PdL^2** which is further away from the nitrogen bridge. By contrast, the LUMO energy levels of both Pd complexes were similar, because LUMO orbitals are located on the almost equivalent bipyridyl fragments. Such lower energy gap of **PdL^1** suggested better absorption of low-energy light, which explains the observed differences in the UV-vis spectra of the two isomers. These results were confirmed by time-dependent density functional theory calculations (TDDFT) for both complexes in methanol, using COSMO to simulate solvent effects (Fig. S14 left). The calculated spectrum of **PdL^1** (Figure AI.6, left) showed lower energy (515 nm) for the HOMO-LUMO transition, compared to **PdL^2** (449 nm). These transition energies were decreased (404 and 367 nm, respectively) by protonation of the nitrogen bridge (Figure AI.6, right), which may happen in the slightly acidic environment of cancer cells; however, the trend between [**PdHL^1**]$^+$ and [**PdHL^2**]$^+$ was identical to that seen for **PdL^1** and **PdL^2**. Overall, calculations clearly demonstrated that a change of the position of the carbon-metal bond had a strong influence on the HOMO-LUMO energy gaps of these cyclometalated palladium complexes.

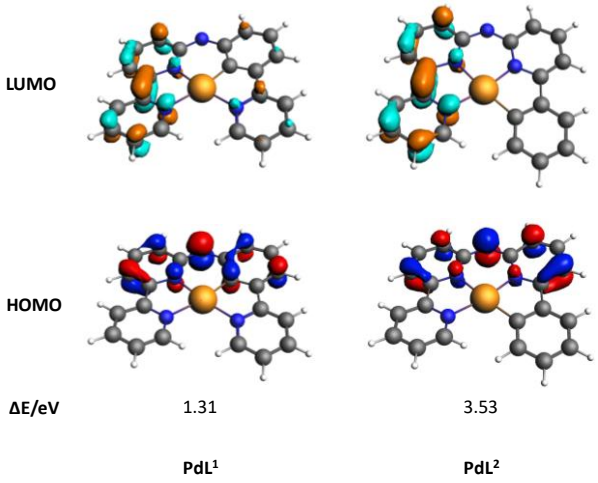

Figure 2.3 *DFT calculation of HOMOs (bottom) and LUMOs (top) orbitals of* ***PdL^1*** *and* ***PdL^2****; occupied orbitals (HOMO) have red and blue lobes, and unoccupied orbitals (LUMO) brown and cyan lobes. Element colour code: grey = C; orange = Pd; blue = N; white = H.*

2.3 Conclusion

In summary, the new cyclopalladated complex **PdL^1** showed good absorbance in the blue region of the spectrum, low phosphorescence, and excellent singlet oxygen quantum yield (0.89), which altogether translated into high photoindex in human cancer cells. By contrast, its isomer **PdL^2** had low absorption and low singlet oxygen quantum yield (0.38), resulting in negligible activation by blue light *in vitro*. DFT calculation showed that the higher absorption in the blue region of **PdL^1**, and thus its lower HOMO-LOMO energy gap, was due to the closer proximity between the electron-rich cyclometalated aromatic cycle and the nitrogen bridge of the ligand, while in **PdL^2** both aromatic rings adjacent to the N bridge are electron-poor pyridine rings, which lowers the HOMO energy. To the best of our knowledge, this study is the first report that two isomers of organometallic prodrugs have distinct photobiological properties. These results demonstrate that changing the position of the carbon-metal bond in the coordination sphere of photoactive organometallic prodrugs can be used to tune the energy gap between their frontier orbitals, and hence their absorption in the visible region of the spectrum.

2.4 Experimental section

2.4.1 materials and methods

All syntheses were performed in a dinitrogen atmosphere. All the chemical compounds were purchased from Sigma-Aldrich. All reactants and solvents were used without further purification. All ^{1}H NMR, ^{13}C attached-proton-test NMR (^{13}C-APT NMR) were recorded on a Bruker DPX-300 or DMX-400 spectrometers. Chemical shifts are indicated in ppm relative to the residual solvent peak. Electrospray ionization mass spectra (ESI-MS) were recorded by using a MSQ Plus Spectrometer positive ionization mode. High-resolution mass spectra (HRMS) of two palladium complexes were recorded on Waters XEVO-G2 XSQ-TOF) mass spectrometer equipped with an electrospray ion source in positive mode (source voltage 3.0 kV, desolvation gas flow 900 L/hr, temperature 250 °C) with resolution R = 22000 (mass range m/z = 50-2000) and 200 pg/uL Leu-enkephalin (m/z = 556.2771) as a “lock mass”. Uv-vis spectra were recorded on a Cary 50 spectrometer from Varian. The singlet oxygen spectra and phosphorescence quantum yield were measured on a special custom-built setup which was described previously. The phosphorescence lifetime of complexes in methanol was measured by LifeSpec-II from Edinburgh Instruments, with excitation source of 375 nm pulsed diode lasers. The partition coefficient log P_{ow} was measured by ICP-OES using a Vista-MPX CCD Simultaneous ICP-OES. The DFT calculations were carried out using the Amsterdam Density

Functional software (ADF2017) from SCM, the PBE0 functional, a triple zeta basis set (TZP), and COSMO to simulate the solvents effects in methanol. Human cancer cell line A549 (human lung carcinoma) and A431 (human skin carcinoma) were purchased from Sigma Aldrich, distributed by the European Collection of Cell Cultures (ECACC). Dulbecco's Modified Eagle Medium (DMEM, with and without phenol red, without glutamine), Glutamine-S (GM; 200 mm), tris(hydroxylmethyl)aminomethane (Tris base), trichloroacetic acid (TCA), glacial acetic acid, and sulfo-rhodamine B (SRB) were purchased from Sigma Aldrich. The measurements of complexes on photocytotoxicity were performed according to the literature.

2.4.2 Synthesis

2-(3-Aminophenyl)pyridine.

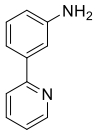

This compound was synthesized according to a modified literature procedure.[3] To a suspension of 2-bromopyridine (0.8 mL, 8.2 mmol), 3-aminophenylboronic acid (1.1 g, 7.7 mmol), anhydrous K_2CO_3 (2.1 g, 15.4 mmol) and $Pd(PPh_3)_4$ (431 g, 0.4 mmol) in 1 ,2-dimethoxyethane (19 mL) under N_2, ethanol (6 mL) and water (13 mL) were added. The mixture was refluxed under N_2 at 95 °C for 24 h. It was allowed to cool and filtered, then water (100 mL) and EtOAc (100 mL) were added. The phases were separated and the aqueous phase was extracted with EtOAc (100 mL) three times. The combined organic phases were dried over Na_2SO_4 and the solvent was rotary evaporated. The crude product obtained was purified by silica chromatography using pentane-EtOAc mixtures (2:1, R_f = 0.35) as eluent, to afford 1.0 g of the target compound (yield: 77%, 5.9 mmol). **ESI-MS** (cation): m/z calcd 171.1 ($C_{11}H_{10}N_2$ + H^+), found 171.1. **^{1}H NMR** (300 MHz, $CDCl_3$): δ 8.69 (1 H, dt, *J* = 4.9, 1.4 Hz), 7.72 – 7.64 (2 H, m), 7.40 (1 H, t, *J* = 2.0 Hz), 7.36 (1 H, dt, *J* = 7.6, 1.4 Hz), 7.26 (1 H, s), 7.22 – 7.18 (1 H, m), 7.17 (0 H, d, *J* = 2.8 Hz), 6.73 (1 H, ddd, *J* = 7.9, 2.5, 1.1 Hz), 3.89 (2 H, s).

H_2L^1 (N-(3-(pyridin-2-yl)phenyl)-[2,2'-bipyridin]-6-amine).

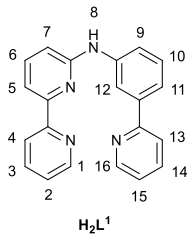

H_2L^1

A mixture of 6-bromo-2,2'-bipyridine (665 mg, 2.8 mmol), $Pd(dba)_2$ (30 mg, 0.5 mmol), racemic 2,2′-bis(diphenylphosphino)-1,1′-binaphthyl (BINAP, 61.4 mg, 0.098 mmol) and KO*t*-Bu (997 mg, 8.9 mmol) was partially dissolved in dry toluene (53 mL) under N_2 atmosphere.[4] The mixture was stirred for 10 min, then 2-(3-Aminophenyl)pyridine (484 mg, 2.8 mmol) was added, followed by heating the reaction mixture to 85 °C. After 3 days stirring, the brown mixture was cooled down. Demi water (75.0 mL) was added and the mixture was stirred for 1 h. The mixture was then filtered, but no solids were obtained. The H_2O layer was separated from the toluene

layer. Extracted the H_2O layer with EtOAc (100 mL) for three times and combined the toluene and EtOAc layers, followed by rotary evaporation of the solvents. The crude product obtained was purified by silica chromatography using pentane-EtOAc mixtures (2:1, R_f = 0.25) as eluent, to afford 67.1 mg of the target compound **H_2L^1** (yield: 73%, 0.21 mmol). **ESI-MS** (cation): m/z calcd 325.1 ($C_{21}H_{16}N_4 + H^+$), found 325.4. **^{1}H NMR** (300 MHz, DMSO-d_6): 9.40 (1 H, s, H^8), 9.03 (1 H, t, *J* = 2.0 Hz, H^{12}), 8.75 (1 H, ddd, *J* = 4.8, 1.8, 1.0 Hz, H^1), 8.68 (1 H, ddd, *J* = 4.7, 1.9, 0.9 Hz, H^{16}), 8.61 (1 H, dt, *J* = 8.0, 1.1 Hz, H^4), 8.01 – 7.97 (1 H, m, H^{14}), 7.96 (1 H, d, *J* = 1.4 Hz, H^{13}), 7.91 (1 H, td, *J* = 7.6, 1.8 Hz, H^3), 7.84 (1 H, dd, *J* = 7.5, 0.9 Hz, H^5), 7.74 (1 H, t, *J* = 7.8 Hz, H^6), 7.68 (1 H, ddd, *J* = 8.1, 2.3, 1.0 Hz, H^9), 7.60 (1 H, dt, *J* = 7.9, 1.2 Hz, H^{11}), 7.48 – 7.44 (1 H, m, H^{10}), 7.43 (1 H, d, *J* = 4.5 Hz, H^5), 7.41 – 7.35 (1 H, m, H^2), 6.93 (1 H, dd, *J* = 8.2, 0.9 Hz, H^7). **^{13}C-APT NMR** (75 MHz, DMSO-d_6), δ 156.9, 156.2, 155.8, 153.6, 150.0, 149.6, 142.6, 139.6, 138.7, 137.6, 129.5, 124.3, 123.1, 121.0, 120.6, 119.0, 118.9, 116.6, 112.2, 111.6.

H_2L^2 (N-(6-phenylpyridin-2-yl)-[2,2'-bipyridin]-6-amine).

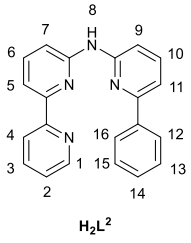

H_2L^2

A mixture of 6-bromo-2,2'-bipyridine (665 mg, 2.8 mmol), $Pd(dba)_2$ (30 mg, 0.5 mmol), racemic BINAP (61 mg, 0.1 mmol) and KO*t*-Bu (997 mg, 8.9 mmol) was partially dissolved in 53 mL dry toluene under N_2 atmosphere.[4] The mixture was stirred for 10 min, then 2-Amino-6-phenylpyridine (484 mg, 2.8 mmol) was added, followed by heating the reaction mixture to 85 °C. After 3 days of stirring, the brown mixture was cooled down with an ice bath. Demi water (75.0 mL) was added and the mixture was stirred for 1 h. The mixture was filtered, but no solids were obtained. The H_2O layer was separated from the toluene layer. Extracted the H_2O layer with EtOAc (100 mL) three times and combined the toluene and EtOAc layers, followed by the evaporation of solvents. The residues were dissolved in EtOAc and recrystallized at -20 °C, to get 596 mg of the target compound **H_2L^2** (yield: 65%, 1.8 mmol). **ESI-MS** (cation): m/z calcd 325.1 ($C_{21}H_{16}N_4 + H^+$), found 325.5. **^{1}H NMR** (400 MHz, DMSO-d_6) 9.86 (1 H, s, H^8), 8.69 (1 H, ddd, *J* = 4.7, 1.8, 0.9 Hz, H^1), 8.38 (1 H, dt, *J* = 7.9, 1.1 Hz, H^4), 8.13 – 8.07 (2 H, m, H^{13}, H^{14}), 7.99 (1 H, td, *J* = 7.7, 1.8 Hz, H^3), 7.95 – 7.79 (5 H, m, H^{10}, H^9, H^7, H^{16}, H^5), 7.54 – 7.41 (5 H, m, H^2, H^6, H^{11}, H^{12}, H^{15}). δ **^{13}C-APT NMR** (101 MHz, DMSO-d_6) δ 155.6, 154.4, 154.09, 154.0, 153.4, 149.3, 139.0, 138.8, 138.7, 137.3, 129.0, 128.8, 126.6, 124.1, 120.4, 112.8, 112.5, 112.4, 110.7.

PdL^1

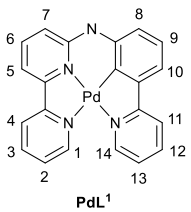

PdL¹

A mixture of **H₂L¹** (36 mg, 0.1 mmol) and $Pd(OAc)_2$ (25 mg, 0.1 mmol) in a glacial acetic acid was refluxed for 12 h at 135 °C under N_2 atmosphere to give a yellowish green solution. Then the solvent was rotary evaporated. The resulted yellow solid was washed with EtOAc, ether and dried in vacuum to get 43 mg of pure **PdL¹** complex (yield: 92%, 0.1 mmol). **HRMS** (cation): m/z calcd 429.0326 ($C_{21}H_{14}N_4Pd + H^+$), found 429.0339. **¹H NMR** (400 MHz, Methanol-d_4) δ 8.34 (1 H, d, J = 5.4 Hz, H^1), 8.20 (1 H, d, J = 8.1 Hz, H^4), 8.14 (1 H, d, J = 5.6 Hz, H^{14}), 8.12 – 8.05 (1 H, m, H^3), 7.93 (1 H, td, J = 7.9, 1.4 Hz, H^{12}), 7.72 (2 H, dd, J = 8.1, 6.1 Hz, H^6, H^{11}), 7.58 (2 H, d, J = 7.3 Hz, H^2, H^5), 7.26 (1 H, t, J = 6.5 Hz, H^{13}), 7.15 (1 H, d, J = 7.4 Hz, H^{10}), 7.08 (1 H, t, J = 7.6 Hz, H^9), 7.02 (1 H, d, J = 8.5 Hz, H^7), 6.73 (1 H, d, J = 7.7 Hz, H^8). **¹³C** NMR (101 MHz, Methanol-d_4) δ 165.9 (**Pd-C**), 155.6, 153.3, 149.7, 148.7, 147.6, 146.4, 141.1, 140.7, 138.7, 137.1, 134.6, 127.8, 127.3, 124.5, 124.0, 121.2, 119.9, 118.4, 117.6, 115.2. **Elemental analysis** calcd for **PdL¹** + $2H_2O$ + CH_3COOH: C, 52.63; H, 4.23; N, 10.67; Found for **PdL¹** + $2H_2O$ + CH_3COOH: C, 52.21; H, 4.42; N, 10.43.

PdL²

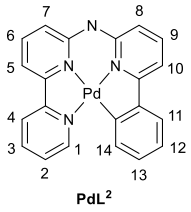

PdL²

The synthesis of complex **PdL²** was similar to that of **PdL¹**, except that ligand **H₂L²** was used. A mixture of **H₂L²** (32 mg, 0.1 mmol) and $Pd(OAc)_2$ (22 mg, 0.1 mmol) in a glacial acetic acid was refluxed for 12 h at 135 °C under N_2 atmosphere to give a yellowish green solution. Then the solvent was rotary evaporated. The resulted yellow solid was washed with EtOAc, ether and dry in vacuum to get 41 mg of pure **PdL²** complex (yield: 95%, 0.1 mmol). The red rectangular single crystal of **PdL²** was obtained by slow evaporation of ether into a saturated methanol solution of **PdL²**. **HRMS** (cation): m/z calcd 429.0326 ($C_{21}H_{14}N_4Pd + H^+$), found 429.0337. **¹H NMR** (400 MHz, Methanol-d_4) δ 8.05 (1 H, d, J = 5.6 Hz, H^1), 7.80 – 7.65 (2 H, m, H^3, H^4), 7.53 (1 H, t, J = 7.9 Hz, H^6, H^9), 7.45 (1 H, t, J = 7.8 Hz, H^5), 7.25 (1 H, d, J = 7.5 Hz, H^2), 7.17 (1 H, t, J = 6.3 Hz, H^{11}), 6.99 (1 H, d, J = 7.6 Hz, H^{10}), 6.87 (1 H, d, J = 7.6 Hz, H^7), 6.80 (2 H, t, J = 7.2 Hz, H^{12}), 6.74 – 6.65 (1 H, m, H^{13}), 6.55 (1 H, d, J = 8.2 Hz, H^8), 6.49 (1 H, d, J = 7.6 Hz, H^{14}). **¹³C** NMR (101 MHz, Methanol-d_4) δ 162.27 (**Pd-C**), 156.0, 154.3, 149.4, 148.8, 146.7, 145.7, 145.6, 139.1, 138.8, 138.8, 129.9, 128.4, 125.8, 124.8, 123.4, 122.8, 116.4, 114.9, 112.7, 111.2. **Elemental analysis** calcd for **PdL²** + H_2O + MeOH: C, 55.18; H, 4.21; N, 11.70; Found for **PdL²** + H_2O + MeOH: C 55.13; H 4.22; N 11.15.

2.4.3 Single-crystal X-ray crystallography

All reflection intensities were measured at 110(2) K using a SuperNova diffractometer (equipped with Atlas detector) with Mo *K*α radiation (λ = 0.71073 Å) under the program CrysAlisPro (Version CrysAlisPro 1.171.39.29c, Rigaku OD, 2017). The same program was used to refine the cell dimensions and for data reduction. The structure was solved with the program SHELXS-2014/7 (Sheldrick, 2015) and was refined on F^2 with SHELXL-2014/7. Numerical absorption correction based on gaussian integration over a multifaceted crystal model was applied using CrysAlisPro. The temperature of the data collection was controlled using the system Cryojet (manufactured by Oxford Instruments). The H atoms were placed at calculated positions using the instructions AFIX 43 with isotropic displacement parameters having values 1.2 *U*eq of the attached C atoms. The structure is disordered. The whole Pd complex is disordered over two orientations as both orientations may have the same space filling requirement. The occupancy factor of the major component of the disorder refines to 0.835(3).

2.4.4 Partition coefficients (log P_{ow}) of palladium complexes

The partition coefficients of palladium complexes were determined by the shake-flask method. Briefly, each palladium complex was dissolved (0.8 mM) in octanol-saturated water and ultrasonicated for 1 h. After filtering with 0.2 µM membrane filters, aliquots of the stock solutions (0.2 mL) were transferred to 15 mL centrifuge tubes and diluted up to 6.0 mL. Then 6.0 mL of water-saturated octanol was added to one of the tubes and the mixture was shaken in a IKA Vibrax shaker for 24 h at 2200 pm. The mixture was then centrifuged for 20 min at 4300 rpm to separate the water phase. For each of the samples, a 5.5 mL aliquot of the aqueous layer was taken using a syringe and 65% HNO_3 (vol) was added to it to give diluted samples with 5% HNO_3 final concentration. The palladium concentrations $[Pd]_{aq}$ (in ppm) of the samples were determined by ICP-OES using a Vista-MPX CCD Simultaneous ICP-OES. Partition coefficients log P_{ow} was calculated using the equation below:

$$\log P_{ow} = \log ([Pd]_{oct}/[Pd]_{aq}) = \log ([Pd]_{total} - [Pd]_{aq}) /[Pd]_{aq}$$

where $[Pd]_{total}$ is the concentration of palladium in the sample that was not extracted with octanol, and $[Pd]_{aq}$ is the concentration of palladium in the aqueous layer after octanol addition, as a mean of three replicates.

2.4.5 Cell culturing

Cells were thawed and at least passaged twice before starting photocytotoxicity experiments. Cells were cultured in DEMEM complete medium (Dulbecco's Modified Eagle Medium

(DMEM) with phenol red, supplemented with 8.0% v/v fetal calf serum (FCS), 0.2% v/v penicillin/streptomycin (P/S), and 0.9% v/v Glutamine), under humidified normoxic conditions, 37 °C atmosphere, 21% O_2 and 7.0% CO_2 in 75 cm^2 flasks. They were sub-cultured upon reaching 70-80% confluence, approximately once per week. Cells were passaged never more than 8 weeks.

2.4.6 Cytotoxicity assay

The cell irradiation system consists of a Ditabis thermostat (980923001) fitted with two flat-bottom microplate thermoblocks (800010600) and a 96-LED array fitted to a standard 96-well plate. The 455 nm LED (FNL-U501B22WCSL), fans (40 mm, 24 V DC, 9714839), and power supply (EA-PS 2042-06B) were ordered from Farnell. Full description of the cell irradiation setup is given in Hopkins et al.[2] The cytotoxicity of **PdL^1** and **PdL^2** were assayed in normoxic conditions (21 % O_2) against two human cancer cell lines (A549 and A431) according to a published protocol. Briefly, 24 h after seeding, the cells were treated with **PdL^1** and **PdL^2** with a range of 6 different concentrations (0, 0.625, 3.125, 6.25, 12.5, 31.25, 62.5 μM, maximum 0.5% DMSO was used in each well). After 24 h incubation, one plate was irradiated with blue light (455 nm, 5 min, 10.5 mW cm^{-2}, 3.2 J cm^{-2}) while the other was left in the dark. Cell viability was then assayed 96 h after seeding using standard sulforhodamine B (SRB) assay. Half maximal effective concentrations (EC_{50}) for cell growth inhibition were calculated by fitting the curves using a non-linear regression function for the dose-response curves of treated vs. non-treated wells via Graphpad prism 5.

$$100/(1 + 10^{log_{10}EC_{50} - X) \times Hill\ Slope})$$

2.4.7 Singlet oxygen generation and phosphorescence quantum yield

The quantum yields of singlet oxygen generation and phosphorescence were determined in a custom-built setup shown in Scheme S2. All optical parts were connected with optical fibers from Avantes, with a diameter of 200–600 μm. The sample, consisting of the compound in deuterated methanol (500 μL), was added to a 104F-OS semi-micro fluorescence cuvette from Hellma Analytics, and placed in a CUV-UV/VIS-TC temperature-controlled cuvette holder (Avantes). The sample was allowed to equilibrate at 298 K for 5 minutes. Emission spectroscopy was performed with a 450 nm fiber-coupled laser (LRD-0450, Laserglow), which was set to 50 mW at the cuvette (4 mm beam diameter; 0.4 W·cm^{-2}) at a 90° angle with respect to the spectrometer. The excitation power was measured using a S310C thermal sensor connected to a PM100USB power meter (Thorlabs). The emission spectra were recorded using

two separate spectrometers for the UV-Vis and NIR emission, *i.e.* from 300 nm to 1000 nm for the phosphorescence of the complex (Avantes 2048L StarLine spectrometer) and from 1000 nm to 1700 nm for the phosphorescence of singlet oxygen ($^1\Delta_g$) around 1275 nm (Avantes NIR256-1.7TEC spectrometer, detector set to −12 °C). The infrared emission spectrum was acquired within 9 seconds, after which the laser was turned off directly. Similarly, the visible emission spectrum was acquired within 2 seconds. UV-Vis absorption spectra before and after emission spectroscopy were measured using an Avalight-DHc halogen-deuterium lamp (Avantes) as light source (turned off during emission spectroscopy) and the before mentioned UV-Vis spectrometer as detector, both connected to the cuvette holder at a 180° angle. All spectra were recorded using Avasoft 8.5 software from Avantes and further processed using Microsoft Office Excel 2010 and Origin Pro 9.1 software. The quantum yields of phosphorescence and singlet oxygen production were calculated using the relative method with **[Ru(bpy)$_3$]Cl$_2$** as the standard (Φ_Δ = 0.73, Φ_P = 0.015 in MeOD), according to Equation below:

$$\Phi_{\mathrm{sam}} = \Phi_{\mathrm{std}} \times \frac{A_{\mathrm{std}}^{450}}{A_{\mathrm{sam}}^{450}} \times \frac{E_{\mathrm{sam}}}{E_{\mathrm{std}}}$$

where Φ is the quantum yield, A^{450} is the absorbance at 450 nm (always kept below 0.1 for a 4 mm path length), E is the integrated emission peak of singlet oxygen at 1270 nm or the integrated phosphorescence emission peak between 520 and 950 nm, and *sam* and *std* denote the sample and standard, respectively.

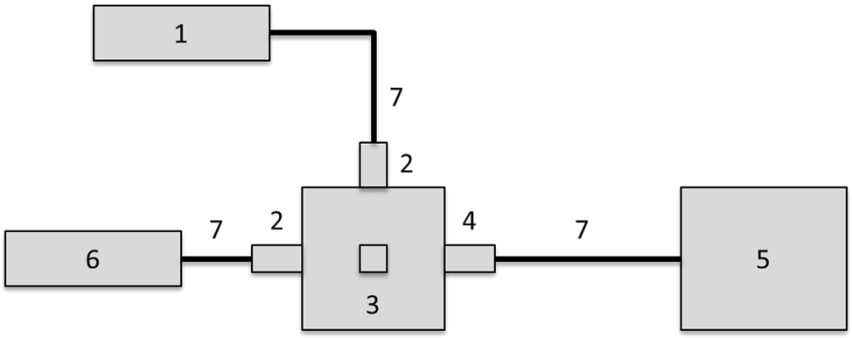

Scheme 2.2 *Setup used for Φ_Δ and Φ_P determination. (1) 450-nm CW laser light source, (2) collimating lens, (3) temperature-controlled cuvette holder, (4) double collimator, (5) UV-Vis (300-1000 nm) or NIR (1000-1700 nm) CCD spectrometer, (6) UV-Vis halogen-deuterium light source, and (7) optical fibers.*

2.5 Acknowledgement

X. Zhou gratefully acknowledges the China Scholarship Council (CSC) for a personal grant (No. 201606200045). This work is supported by an ERC Starting Grant to S. Bonnet.

2.6 References

1. T. C. Johnstone, K. Suntharalingam and S. J. Lippard, *Chem. Rev.*, 2016, **116**, 3436-3486.
2. L. Kelland, *Nat. Rev. Cancer*, 2007, **7**, 573-584.
3. D. Wang and S. J. Lippard, *Nat. Rev. Drug Discovery*, 2005, **4**, 307-320.
4. L. Ma, N. Wang, R. Ma, C. Li, Z. Xu, M. K. Tse and G. Zhu, *Angew. Chem. Int. Ed.*, 2018, **57**, 1-6.
5. S. Medici, M. Peana, V. M. Nurchi, J. I. Lachowicz, G. Crisponi and M. A. Zoroddu, *Coord. Chem. Rev.*, 2015, **284**, 329-350.
6. N. Cutillas, G. S. Yellol, C. de Haro, C. Vicente, V. Rodriguez and J. Ruiz, *Coord. Chem. Rev.*, 2013, **257**, 2784-2797.
7. L. Zeng, P. Gupta, Y. Chen, E. Wang, L. Ji, H. Chao and Z. S. Chen, *Chem. Soc. Rev.*, 2017, **46**, 5771-5804.
8. F. E. Poynton, S. A. Bright, S. Blasco, D. C. Williams, J. M. Kelly and T. Gunnlaugsson, *Chem. Soc. Rev.*, 2017, **46**, 7706-7756.
9. H. Huang, P. Zhang, H. Chen, L. Ji and H. Chao, *Chem. Eur. J.*, 2015, **21**, 715-725.
10. T. T. Fong, C. N. Lok, C. Y. Chung, Y. M. Fung, P. K. Chow, P. K. Wan and C. M. Che, *Angew. Chem. Int. Ed.*, 2016, **55**, 11935-11939.
11. M. Fanelli, M. Formica, V. Fusi, L. Giorgi, M. Micheloni and P. Paoli, *Coord. Chem. Rev.*, 2016, **310**, 41-79.
12. A.-R. Azzouzi, S. Vincendeau, E. Barret, A. Cicco, F. Kleinclauss, H. G. van der Poel, C. G. Stief, J. Rassweiler, G. Salomon, E. Solsona, A. Alcaraz, T. T. Tammela, D. J. Rosario, F. Gomez-Veiga, G. Ahlgren, F. Benzaghou, B. Gaillac, B. Amzal, F. M. J. Debruyne, G. Fromont, C. Gratzke and M. Emberton, *Lancet Oncol.*, 2017, **18**, 181-191.
13. H. Cao, L. Wang, Y. Yang, J. Li, Y. Qi, Y. Li, Y. Li, H. Wang and J. Li, *Angew. Chem. Int. Ed.*, 2018, **57**, 7759-7763.
14. Y. Ma, X. Li, A. Li, P. Yang, C. Zhang and B. Tang, *Angew. Chem. Int. Ed.*, 2017, **56**, 13752-13756.
15. S. H. Askes, A. Bahreman and S. Bonnet, *Angew. Chem. Int. Ed.*, 2014, **53**, 1029-1033.
16. S. L. Higgins and K. J. Brewer, *Angew. Chem. Int. Ed.*, 2012, **51**, 11420-11422.
17. H. Bi, Y. Dai, P. Yang, J. Xu, D. Yang, S. Gai, F. He, B. Liu, C. Zhong, G. An and J. Lin, *Small*, 2018, **14**, e1703809.
18. H. Bi, Y. Dai, P. Yang, J. Xu, D. Yang, S. Gai, F. He, G. An, C. Zhong and J. Lin, *Chem. Eng. J. (Lausanne)*, 2019, **356**, 543-553.
19. J. D. Knoll and C. Turro, *Coord. Chem. Rev.*, 2015, **282-283**, 110-126.
20. F. Heinemann, J. Karges and G. Gasser, *Acc. Chem. Res.*, 2017, **50**, 2727-2736.
21. J.-Y. Lee, J.-Y. Lee, Y.-Y. Chang, C.-H. Hu, N. M. Wang and H. M. Lee, *Organometallics*, 2015, **34**, 4359-4368.
22. S. M. Ray, R.; Singh, J. K.; Samantaray, M. K.; Shaikh, M. M; Panda, D.; Ghosh, P, *J. Am. Chem. Soc.*, 2007, 15042-15053.
23. S. G. Churusova, D. V. Aleksanyan, E. Y. Rybalkina, O. Y. Susova, V. V. Brunova, R. R. Aysin, Y. V. Nelyubina, A. S. Peregudov, E. I. Gutsul, Z. S. Klemenkova and V. A. Kozlov, *Inorg. Chem.*, 2017, **56**, 9834-9850.
24. W. Liu and R. Gust, *Chem. Soc. Rev.*, 2013, **42**, 755-773.
25. J. Ruiz, V. Rodriguez, C. de Haro, A. Espinosa, J. Perez and C. Janiak, *Dalton Trans.*, 2010, **39**, 3290-3301.
26. G. Gasser, I. Ott and N. Metzler-Nolte, *J. Med. Chem.*, 2011, **54**, 3-25.
27. S. Bonnet, *Comments Inorg. Chem.*, 2014, **35**, 179-213.
28. Z. Fan, J. Ni and A. Zhang, *J. Am. Chem. Soc.*, 2016, **138**, 8470-8475.
29. V. H. S. van Rixel, B. Siewert, S. L. Hopkins, S. H. C. Askes, A. Busemann, M. A. Siegler and S. Bonnet, *Chem. Sci.*, 2016, **7**, 4922-4929.
30. E. M. Hernández, S. Zheng, H. J. Shepherd, D. S. Yufit, K. Ridier, S. Bedoui, W. Nicolazzi, V. Velázquez, S. Bonnet, G. Molnár and A. Bousseksou, *J. Phys. Chem. C*, 2016, **120**, 27608-27617.
31. L. Yang, D. R. Powell and R. P. Houser, *Dalton Trans.*, 2007, **0**, 955-964.
32. S. Zheng, N. R. Reintjens, M. A. Siegler, O. Roubeau, E. Bouwman, A. Rudavskyi, R. W. Havenith and S. Bonnet, *Chem. Eur. J.*, 2016, **22**, 331-339.

33. S. L. Hopkins, B. Siewert, S. H. Askes, P. Veldhuizen, R. Zwier, M. Heger and S. Bonnet, *Photochem. Photobiol. Sci.*, 2016, **15**, 644-653.
34. M. C. DeRosa and R. J. Crutchley, *Coord. Chem. Rev.*, 2002, **233-234**, 351-371.
35. X. Li, J. Zhang, Z. Zhao, L. Wang, H. Yang, Q. Chang, N. Jiang, Z. Liu, Z. Bian, W. Liu, Z. Lu and C. Huang, *Adv. Mater.*, 2018, **30**, e1705005.
36. F. F. Hung, S. X. Wu, W. P. To, W. L. Kwong, X. Guan, W. Lu, K. H. Low and C. M. Che, *Chem. Asian J.*, 2017, **12**, 145-158.
37. J. Fernandez-Cestau, B. t. Bertrand, A. Pintus and M. Bochmann, *Organometallics*, 2017, **36**, 3304-3312.